

Antisymmetric Magnetoresistance due to Domain-Wall Tilting in Perpendicularly Magnetized Films


Yangtao Su,^{1,2} Yang Meng^{1,2,*}, Haibin Shi,^{1,2} Li Wang,^{1,2} Xinyu Cao,^{1,2} Ying Zhang,^{1,2} Runwei Li,³
and Hongwu Zhao^{1,2,4,†}

¹*Beijing National Laboratory for Condensed Matter Physics, Institute of Physics, Chinese Academy of Sciences, Beijing 100190, China*

²*School of Physical Sciences, University of Chinese Academy of Sciences, Beijing 100049, China*

³*CAS Key Laboratory of Magnetic Materials and Devices, Ningbo Institute of Materials Technology and Engineering, Chinese Academy of Sciences, Ningbo, Zhejiang 315201, China*

⁴*Songshan Lake Materials Laboratory, Dongguan, Guangdong 523808, China*

 (Received 1 July 2021; revised 18 October 2021; accepted 24 December 2021; published 11 January 2022)

Electrical currents flowing through magnetic domain walls tend to encounter additional extraordinary resistance. At the thin-wall limit, the occurrence of anomalous-field antisymmetric magnetoresistance breaks Onsager symmetry, which seems to be determined by the combination of single-wall and perpendicular-current-injection geometry. However, the delicate magnetic structure and measurement configuration are hard to implement, and the abnormal transport properties observed in multidomain structures are not fully understood. Here, we report the observation of antisymmetric magnetoresistance due to domain-wall tilting in a multidomain structure controlled by a magnetic field gradient. We demonstrate, both experimentally and theoretically, that the anomalous magnetoresistance arises from the nonequilibrium current in the vicinity of tilting domain walls, which are basically governed by the geometry factor of the tilting walls.

DOI: [10.1103/PhysRevApplied.17.014013](https://doi.org/10.1103/PhysRevApplied.17.014013)

I. INTRODUCTION

In a Stoner ferromagnet, when magnetization is homogeneous throughout the material, the magnetoresistance (MR) effect intrinsically originates from the spin-orbit interaction between the spin-polarized current and the magnetic moments [1,2]. Further studies on magnetic heterostructures with controllable magnetization have boosted intriguing and application-oriented discoveries of giant magnetoresistance and tunneling magnetoresistance effects [3–6]. However, when there are inhomogeneities in the magnetization direction, i.e., domain walls, distinct transport processes occur correspondingly, giving rise to various extrinsic anomalous MR [7–11]. Recently, experimental studies have demonstrated that the presence of a single domain wall leads to antisymmetric magnetoresistance in magnetic films with perpendicular anisotropy [12–14]. This phenomenon is attributed to the extraordinary Hall effect induced by circulating currents in the vicinity of the single wall [15–18], where the domain wall, current, and magnetization are mutually perpendicular. However, this “single-wall” model is not applicable

with respect to special criteria for subsequently emerging antisymmetric MR in multidomain structures and in-plane magnetized films [17,19–21]. Indeed, experimental studies on clearly establishing the interplay between the anomalous transport behaviors and particular magnetic domain texture can better help to clarify the origin of the antisymmetric anomaly.

Herein, we report that highly tunable domain-wall tilting can result in antisymmetric MR in perpendicular magnetized multidomain textures. By applying a magnetic field gradient, a spatially inhomogeneous magnetization distribution is realized in $\text{Co}_x\text{Tb}_{1-x}$ films, leading to the magnetoresistance anomaly. We show that the geometry factor of the tilting domain walls governs the formation of nonequilibrium currents, resulting in such anomalous MR in the multidomain structure. The findings further pave the way for designing controllable domain-wall electronic devices.

II. EXPERIMENT

Ferrimagnetic $\text{Co}_x\text{Tb}_{1-x}$ alloys exhibit excellent perpendicular magnetic anisotropy (PMA), and their magnetization reversal is primarily controlled by domain-wall propagation [22,23]. Herein, we use $\text{Co}_{0.85}\text{Tb}_{0.15}$ as a

*ymeng@iphy.ac.cn

†hwzhao@iphy.ac.cn

model material to investigate the effect of inhomogeneous magnetization texture on its transport properties. The Pt(5 nm)/Co_{0.85}Tb_{0.15}(12 nm)/Pt(5 nm) films are deposited on Si substrates by magnetron sputtering. The Co_{0.85}Tb_{0.15} film is prepared by cosputtering Co and Tb targets with adjustable sputtering powers. During film deposition, a metallic mask is used to fabricate the Hall bar structure (width, 5 mm; length, 7 mm; arm width, 0.5 mm). The magnetic properties of Co_{0.85}Tb_{0.15} films are investigated by the magneto-optic Kerr effect (MOKE). The transport measurements are carried out on a physical property measurement system (PPMS-9) and a Janis ST-300 cryostat, respectively, where the magnetoresistance ($\Delta R/R_{xx}(H=0) = [R_{xx}(H) - R_{xx}(H=0)]/[R_{xx}(H=0)]$) and transverse Hall resistance, R_H , are simultaneously measured. Using an EVICO Kerr microscope, the magnetic domain structures are simultaneously characterized during magnetic transport measurements. The magnetic field, H , is always applied normal to the film.

III. RESULTS AND DISCUSSION

First, we examine the influence of inhomogeneous magnetization on the transport properties of Co_{0.85}Tb_{0.15}. As shown in the inset of Fig. 1(a), our custom-made electromagnets yield a heterogeneous field with homogeneity below 500 ppm within a cylindrical region of 5 mm in

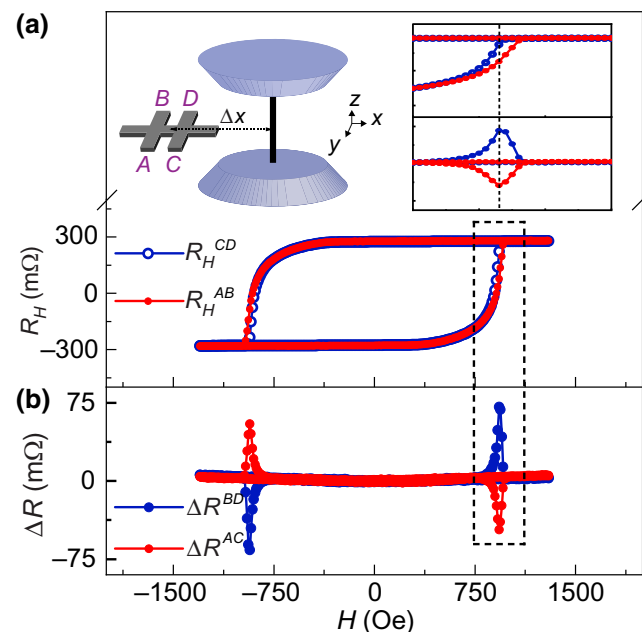


FIG. 1. (a) R_H - H curves in nonuniform field. Left inset, schematic of magnetoresistance measurement configuration. Offset distance is $\Delta x = -13$ mm. Right inset, enlarged views of R_H - H and ΔR - H curves. (b) Asymmetric ΔR in nonuniform field.

radius. Purposely, the Co_{0.85}Tb_{0.15} Hall bar is fixed at an offset position of $\Delta x = -13$ mm, the distance between the centers of magnets and the Hall bar, far away from the region of homogeneous field. As a result, the magnetic field applied at the A - B junction of the Hall bar is actually smaller than that of the C - D junction. The inhomogeneous gradient field directly leads to the slight difference between R_H - H curves measured at A - B and C - D electrode pairs around the saturation field [see the inset of Fig. 1(a)], which is entirely different from the near-zero ΔR obtained in uniform field (see Appendix A). The inconsistency clearly indicates the occurrence of asynchronous magnetization reversals in two Hall junctions. On the other hand, the simultaneously measured magnetoresistance, ΔR , across electrodes A and C exhibits obvious antisymmetric behavior [Fig. 1(b)]. The antisymmetric ΔR - H curves display a negative peak at 930 Oe for the ascending-field branch, and a positive peak at -930 Oe for the descending-field branch. By contrast, ΔR measured across electrodes B and D displays similar antisymmetry but of opposite polarity [Fig. 1(b)]. By carefully comparing ΔR and R_H [see the enlarged views in Fig. 1(a)], it is clearly seen that, when ΔR reaches its maximum, the magnetization of junction C - D is nearly saturated, and the magnetization of junction A - B has not yet occurred. Therefore, the peculiar antisymmetric MR evidently stems from the inhomogeneous magnetization process across two Hall junctions, which is induced by the gradient magnetic field. The antisymmetric MR driven by gradient field is observed in various Hall bars with different film thicknesses, arm widths, and chemical components on different substrates (see Appendix B), thus fully excluding the possibility that the anomalous MR comes from defects in Hall bar structures.

The Hall bar is then delicately relocated at various offset positions along the x axis to experience different magnetic field gradients. The MR across electrodes A and C is measured accordingly, as shown in Fig. 2(a). The negative MR peak of the ascending-field branch is gradually reduced to zero when Δx changes from -13 to 0 mm, and subsequently reverses its sign as Δx changes from 0 to 13 mm. Meanwhile, the positive MR peak of the descending-field branch shows a similar evolutionary trend but of opposite sign. It is easily seen that the MR measured under uniform field ($\Delta x = 0$) is kept nearly zero, which is consistent with the PPMS measurements (see Appendix A). The MR polarity reversal with respect to offset position Δx obviously arises from the opposite spatial distribution of the inhomogeneous gradient field along the x axis. The values of average magnetoresistance, $MR_A = [MR(H) - MR(-H)]/2$, and the peak field at which the MR reaches its maximum of the ascending-field branch, H_M , are derived and plotted as a function of Δx , as shown in Fig. 2(b). While MR_A increases linearly with Δx , H_M remains almost unchanged. The enhanced

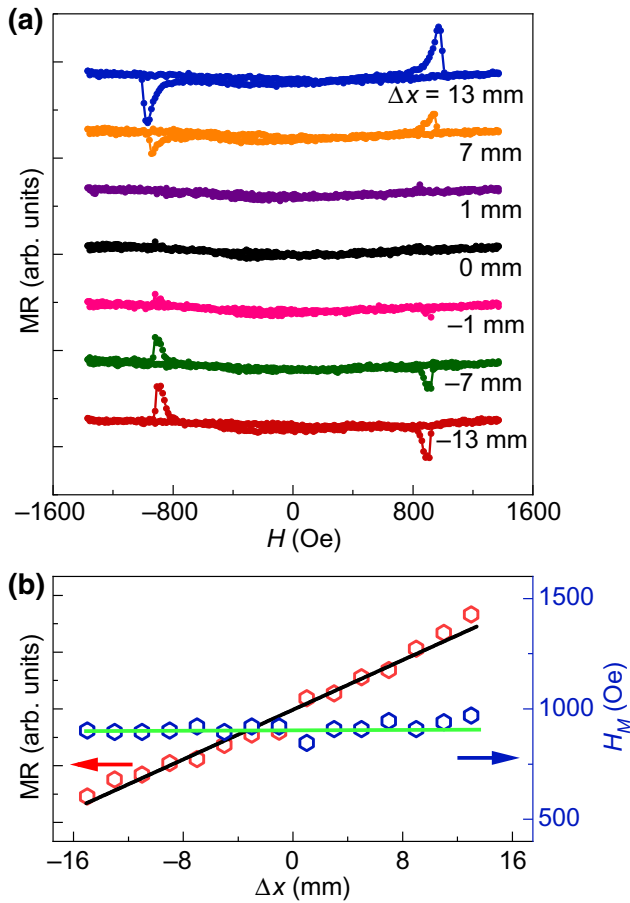


FIG. 2. (a) Antisymmetric MR- H curves measured across electrodes A and C at different offset positions, Δx . (b) Average MR and peak field, H_M , as a function of Δx .

magnetic field gradient apparently leads to a larger magnetoresistance. Thus, these results definitely demonstrate that the antisymmetric MR is triggered by inhomogeneous magnetization reversals across the Hall bar, which can be effectively regulated by altering the inhomogeneous field gradient.

The inhomogeneous magnetization distributions are synchronously characterized by means of MOKE microscopy during transport measurements. For the purpose of reproducing the antisymmetric MR, the sample is intentionally displaced away from the uniform-field region. Figure 3 shows the domain images obtained at selected fields in the ascending-field branch. It is noted that the cross-shaped and wedge-shaped domain patterns appear in the junctions and central-arm regions of the Hall bar, respectively. In the descending-field branch, the domain-pattern evolution exhibits a similar trend with opposite magnetization (see Appendix C). More specifically, the emergence of nonzero MR is closely correlated with the asymmetric distribution of a multidomain texture, which is manifested in the following aspects. (i) The overall area

of the unreversed cross-shaped domain (black) inside junction $A-B$ is generally smaller than that of junction $C-D$, confirming asynchronized magnetization reversal of the two junctions. (ii) In the central-arm region, the wedge-shaped stripe domain with tilting domain walls gradually retreats toward the $C-D$ junction with increasing field until it disappears. (iii) As MR reaches its maximum around 900 Oe, the completely reversed cross-shaped domain within junction $A-B$ contrasts strongly with the mostly unreversed domain within junction $C-D$, while the tip of the wedge-shaped domain shrinks toward the middle of the center arm. Seemingly, both asynchronized magnetization reversal of two junctions and the asymmetric wedge-domain texture in the central arm are associated with the occurrence of antisymmetric MR. It should be noted that these tilting-domain-wall patterns in the arm region of the multiple-domain texture are observed in different samples with various film thickness and structure (see Appendix B). Macroscopically, the inhomogeneous domain texture across the Hall bar is mainly determined by a number of factors. (a) The formation of cross-shaped stripe-domain patterns in junction regions basically stems from competition between shape and crystalline anisotropic energy [24,25], and the field gradient leads to different stripe widths. (b) In the arm region, strong exchange coupling between the lateral stripe-domain texture and that of $A-B$ and $C-D$ junctions subsequently leads to domain-wall tilting. (c) With changing the field gradient, both geometrical restrictions on distinct stripe-domain structures and their exactly matched interconnection result in variation of the tilting geometry. However, the complex distribution of gradient fields is difficult to accurately measure, which severely hampers efforts to define the observed domain patterns from the perspective of micromagnetic simulation. Nevertheless, evolution of the multidomain texture suggests that the single-wall model and perpendicular-current-injection configuration are not simply applicable in our experiment [12,13,16,18].

Based on the experimental domain textures, we calculate the transport properties of the Hall bar, including variation of the electrical potential, φ , and current density, \mathbf{j} , with magnetic field. The current density, \mathbf{j} , is determined by $\mathbf{E} = \rho_{\uparrow\downarrow}\mathbf{j}$, where the resistivity tensor, $\rho_{\uparrow\downarrow} = \begin{pmatrix} \rho_0 & \mp\rho_H \\ \pm\rho_H & \rho_0 \end{pmatrix}$, is determined by the spatial distribution of magnetization, which is directly derived from representative experimental domain data [see Figs. 4(a)–4(d)]. The electrical potential, φ , is related to \mathbf{E} by $\mathbf{E} = -\nabla\varphi$. The extra potential, $\delta\varphi$, and nonequilibrium current, $\delta\mathbf{j}$, caused by the multidomain texture can be defined as $\delta\varphi = \varphi - \varphi_0$ and $\delta\mathbf{j} = \mathbf{j} - \mathbf{j}_0$, where φ_0 and \mathbf{j}_0 represent the electrical potential and current achieved under saturation magnetization, respectively [12,13,16,18].

Figures 4(a)–4(d) show the calculated distributions of $\delta\varphi$ (background color) and $\delta\mathbf{j}$ (black arrows) of the Hall

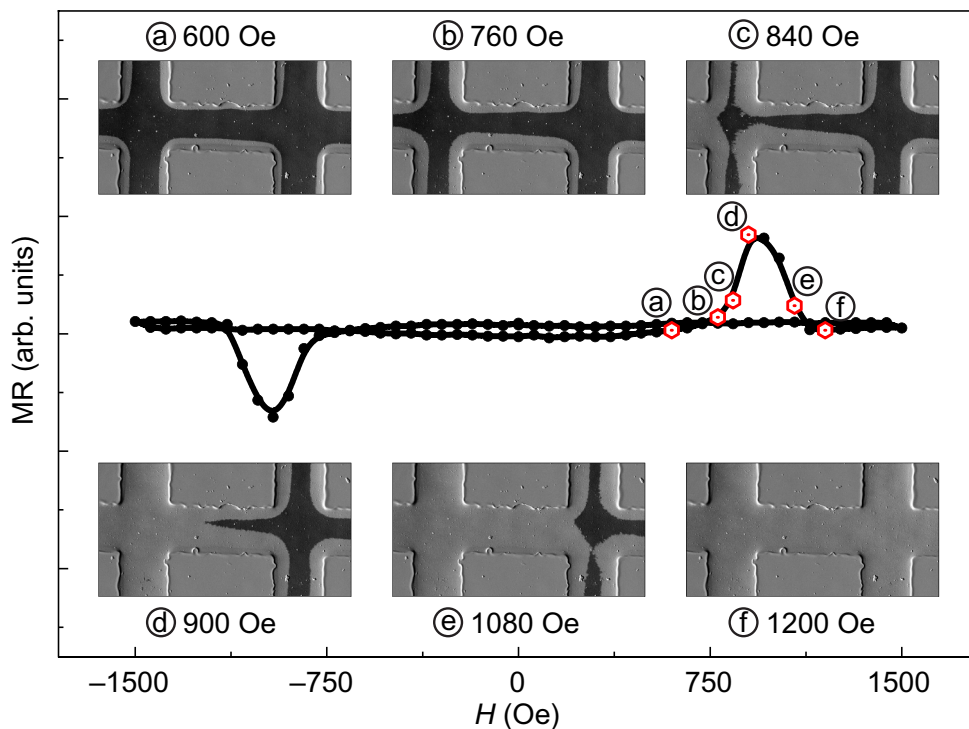


FIG. 3. Field dependence of antisymmetric MR and simultaneously measured MOKE images of domain patterns of the $\text{Co}_{0.85}\text{Tb}_{0.15}$ Hall bar at selected fields.

bar with representative multidomain textures using the commercial software COMSOL. To avoid confusion with the distributions of $\delta\varphi$ and $\delta\mathbf{j}$, the boundaries of the reversed domain walls are simply outlined and superimposed. The nonequilibrium currents, $\delta\mathbf{j}$, not only appear around the cross-shaped domain in junction regions, but also noticeably surround the tilting domain walls in the central-arm region. The enlarged views show that the magnitude of $\delta\mathbf{j}$ in the vicinity of tilting domain walls increases with α , the angle between tilting domain walls. Moreover, the variations of $\delta\varphi$ along the lateral edge of the Hall bar are examined using four probes (V_1 – V_4), see Fig. 4(e). Comparing the distributions of $\delta\varphi$ and $\delta\mathbf{j}$ between different multidomain textures, we can establish the following results. (i) A substantial drop of $\delta\varphi$ occurs between probes V_2 and V_3 , indicating that the antisymmetric MR is mainly determined by the variation of $\delta\varphi$ in the central-arm region. (ii) $\delta\varphi$ changes significantly in the vicinity of tilting domain walls, revealing the dominant role of tilting domain walls in the formation of antisymmetric MR. (iii) With increasing magnetic field, the slope of the $\delta\varphi$ - x curve increases, in line with the enhancement of MR [Fig. 4(f)]. Therefore, the variations of $\delta\varphi$ and $\delta\mathbf{j}$ affected by the domain-wall tilting turn out to be crucial for the occurrence of antisymmetric MR, which contrasts strongly with the special geometries required for experimental observation of the anomalous MR and the single-wall model [12–14,17,18].

To properly describe the effect of domain-wall tilting on nonequilibrium current, we derive the following equation by analytical and numerical calculations (see Appendix D

for detailed calculations):

$$\nabla \times \delta\mathbf{j} = -\frac{j_0 R_s}{\rho_0} \frac{\partial M_z}{\partial x} \hat{\mathbf{k}}, \quad (1)$$

where R_s is the Hall coefficient; M_z and $\hat{\mathbf{k}}$ are the magnetization and unit vector along the normal direction, respectively. Equation (1) reveals that any variations of perpendicular magnetization along the current direction, i.e., tilting domain walls, will directly lead to the emergence of nonequilibrium current $\delta\mathbf{j}$. More specifically, $\delta\mathbf{j}$ associated with tilting walls can be deduced as $|\delta\mathbf{j}| \approx 2j_0(\rho_H/\rho_0) \tan(\alpha/2)$ (see Appendix D), where α is the angle between tilting domain walls. It is obvious that the geometry factor $\tan(\alpha/2)$ is a key parameter for the generation of nonequilibrium currents, which is eventually determined by sample geometry, magnetic anisotropy of films, and the magnetic field gradient in the present study. Based on the derived distribution of $\delta\varphi$ and $\delta\mathbf{j}$ [Figs. 4(a)–4(e)], we further compute MR between electrodes A and B of the Hall bar. As shown in Fig. 4(f), the calculated values of ΔR agree well with experimental results. Thus, our results evidently indicate that the geometry factor of tilting domain walls is essential to produce antisymmetric MR, irrespective of whether the sample contains single- or multiple-domain walls.

IV. CONCLUSION

Our experiments clearly demonstrate that inhomogeneous magnetization driven by a magnetic field gradient gives rise to highly tunable antisymmetric MR in

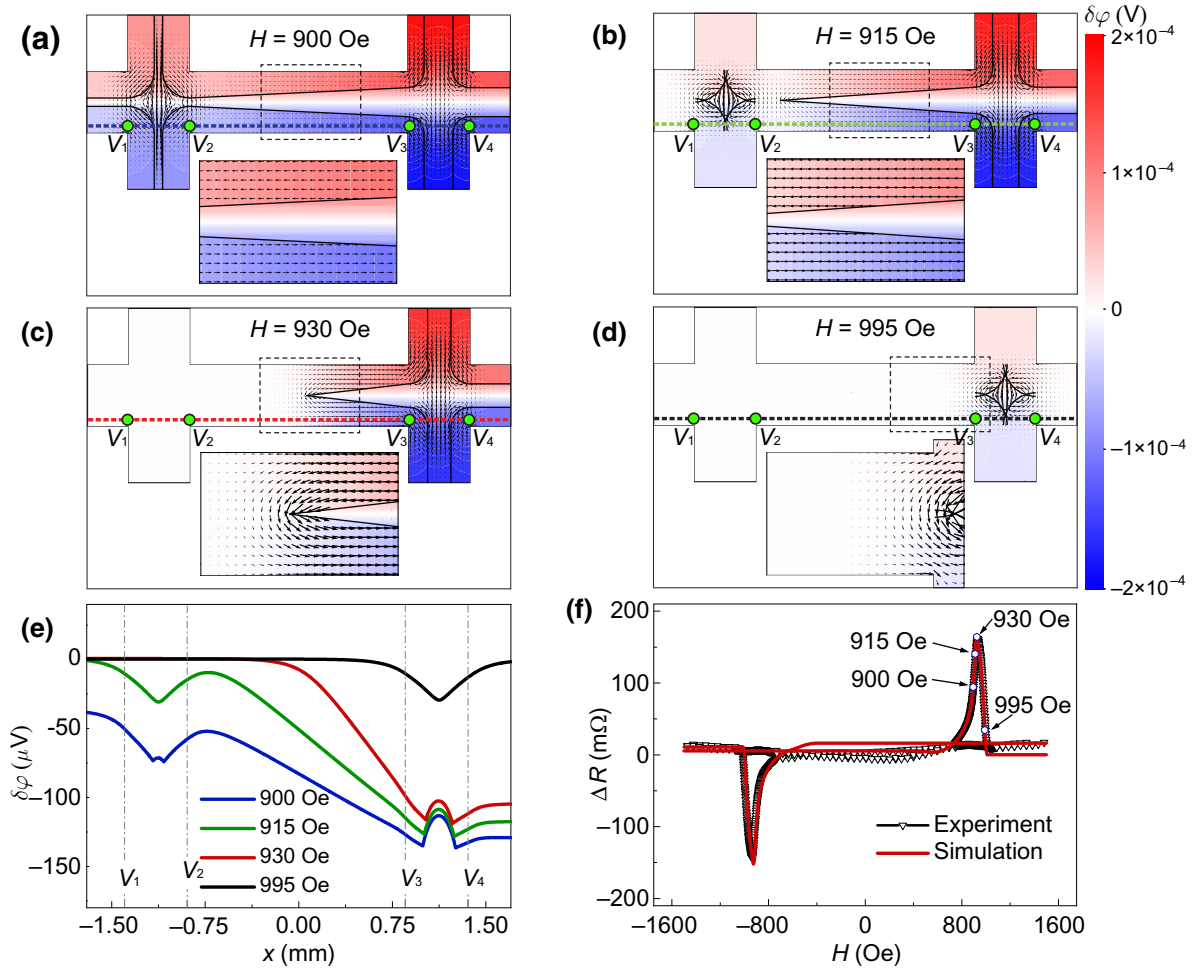


FIG. 4. Distributions of $\delta\varphi$ and $\delta\mathbf{j}$ of the Hall bar with representative multidomain textures under different fields: (a) 900 Oe, (b) 915 Oe, (c) 930 Oe, and (d) 995 Oe. Background color (from red to blue on the scale bar of potential) represents the distribution of $\delta\varphi$. Black arrows represent nonequilibrium currents. Enlarged views of $\delta\mathbf{j}$ ($\times 30$) of selected regions are shown in the inset. (e) Distributions of $\delta\varphi$ along lateral edge of the Hall bar at selected fields. Positions of potential probes are marked as V_1 , V_2 , V_3 , and V_4 . (f) Experimental and calculated ΔR as a function of magnetic field.

$\text{Co}_x\text{Tb}_{1-x}$ films. Delicate control of the magnetic field gradients triggers the formation of inhomogeneous magnetization distribution across the magnetic Hall bar, which makes it possible to tune the antisymmetric MR through regulating the spatial heterogeneity of magnetization. This technique, thus, can be extended to a broad class of ferromagnetic materials, for example, generating multiple-domain walls in in-plane magnetized thin films to induce anomalous transport behavior. Synchronous measurements of the domain structure and transport properties help to explicitly establish the interplay between anomalous transport behavior and particular domain-wall geometries, which is essential to construct a theoretical model and analyze antisymmetric MR. Finally, theoretical calculations show that the induced nonequilibrium current is basically determined by the geometry factor of the tilting-wall texture. Delicate control of MR by properly modulating the geometric parameter demonstrated here provides an

insight into the single-domain-wall-based spin-transport phenomenon.

ACKNOWLEDGMENTS

This work is supported by the National Key Basic Research Project of China (Grant No. 2016YFA0300600), the Strategic Priority Research Program of the Chinese Academy of Sciences (Grant No. XDB33020300), and the National Natural Science Foundation of China (Grants No. 11604375 and No. 11874416).

APPENDIX A: MAGNETIC AND TRANSPORT PROPERTIES OF $\text{Co}_{0.85}\text{Tb}_{0.15}$ UNDER UNIFORM FIELDS

Under uniform magnetic fields, the magnetic and transport properties of the $\text{Co}_{0.85}\text{Tb}_{0.15}$ Hall bar are measured

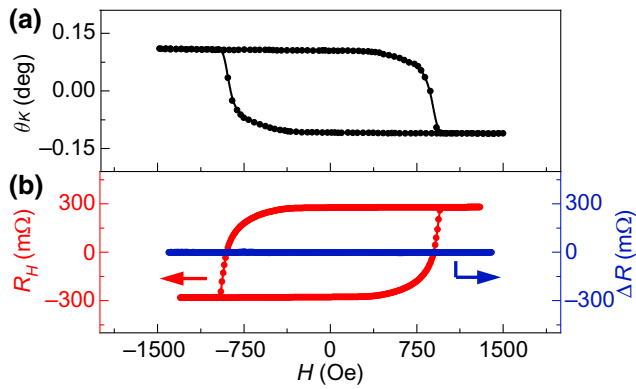


FIG. 5. (a) MOKE hysteresis loop of Pt(5 nm)/Co_{0.85}Tb_{0.15} (12 nm)/Pt(5 nm). (b) Hall resistance, R_H , and magnetoresistance change, ΔR , in uniform magnetic field.

(Fig. 5). The MOKE hysteresis loop shows sharp magnetization reversals with a coercive field, H_c , of around 900 Oe, indicating strong PMA of Co_{0.85}Tb_{0.15} [26]. The transport properties of the Co_{0.85}Tb_{0.15} Hall bar are measured with a PPMS (magnetic field homogeneity <0.01% over 5.5 cm on-axis). Compared with the MOKE hysteresis loop in Fig. 5(a), the Hall resistance, R_H , in Fig. 5(b) shows a similar square shape and the same H_c , revealing that R_H is proportional to magnetization along the field direction. Meanwhile, the simultaneously measured magnetoresistance change, ΔR , is almost zero, resulting from the current-perpendicular-to-magnetization configuration inside magnetic domains and negligible domain-wall magnetoresistance [10,27].

APPENDIX B: ANTISYMMETRIC MR AND DOMAIN PATTERNS OF DIFFERENT STRUCTURES

To confirm that antisymmetric MR results from the inhomogeneous magnetization distribution, instead of defects, such as interface roughness, contract asymmetry,

and uniformity of the film, the Hall bar structures are fabricated on different substrates with various film thicknesses, sizes, and chemical components.

Figure 6 shows representative MR curves of various Hall bars under an inhomogeneous gradient field, clearly indicating that nonuniform magnetization of the Hall bar commonly leads to the antisymmetric MR effect.

Simultaneously, we characterize the domain pattern of Hall bar structures during transport measurements under an inhomogeneous gradient field. Figure 7 depicts representative domain images of different samples, which exhibit clearly tilting domain-wall patterns in the arm region of the multiple-domain texture. Hence, these results doubtlessly demonstrate that antisymmetric MR is closely related to the inhomogeneous magnetization distribution rather than defects in the Hall bars.

APPENDIX C: MAGNETIC DOMAIN EVOLUTION IN DECREASING-FIELD BRANCH

We simultaneously measure the magnetic domain evolution of the Hall bar in the descending-field branch under a gradient magnetic field. As shown in Fig. 8, the cross-shaped patterns and wedge-shaped feature with opposite magnetization to that of the ascending-field branch (Fig. 3) appear in the junctions and central-arm region, respectively. Similar domain evolution with reversed magnetization is clearly presented in the descending-field branch, reconfirming that the emergence of asymmetric MR is closely associated with the inhomogeneous distribution of multidomain textures across the Hall bar structure.

APPENDIX D: CALCULATION OF NONEQUILIBRIUM CURRENT DENSITY

In this section, we give details of our theoretical model, showing that the multidomain texture containing tilting domain walls can generally introduce the nonequilibrium current distribution through analytical and numerical calculations.

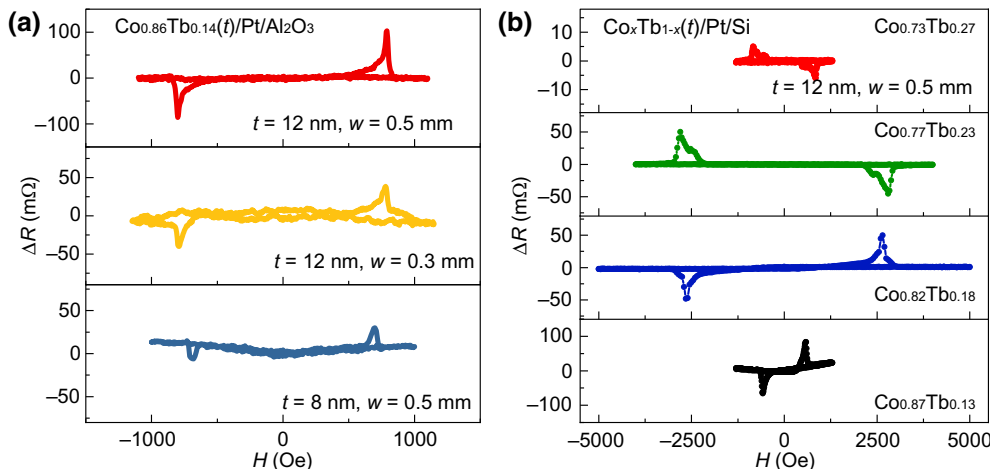


FIG. 6. (a) Field dependence of antisymmetric MR of Co_{0.86}Tb_{0.14} Hall bars with various thicknesses and arm widths. (b) Field dependence of antisymmetric MR of the Hall bars with identical size but different chemical components.

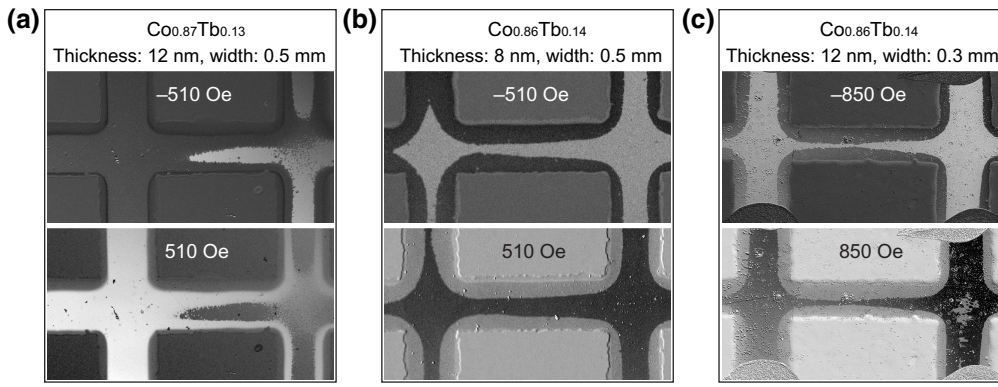


FIG. 7. Typical MOKE images of domain patterns at specified fields of different Hall bar samples. (a) $\text{Co}_{0.87}\text{Tb}_{0.13}$, thickness: 12 nm, width: 0.5 mm. (b) $\text{Co}_{0.86}\text{Tb}_{0.14}$, thickness: 8 nm, width: 0.5 mm. (c) $\text{Co}_{0.86}\text{Tb}_{0.14}$, thickness: 12 nm, width: 0.3 mm.

1. Tilting domain walls inducing nonequilibrium current

We consider a thin magnetic film consisting of two domains with opposite perpendicular magnetization separated by wedge-shaped domain walls (Fig. 9). The film is in the x - y plane and the electric field is applied along the length direction. The electrical field and current density are coupled by Ohm's law:

$$\mathbf{E} = \rho_{\uparrow\downarrow} \mathbf{j}, \quad (\text{D1})$$

where $\rho_{\uparrow\downarrow} = \begin{pmatrix} \rho_0 & -\rho_H \\ \rho_H & \rho_0 \end{pmatrix}$ is the resistivity tensor of the magnetic film. The current density tensor is taken to be $\mathbf{j} = \begin{pmatrix} j_{0x} + \delta j_x \\ j_{0y} + \delta j_y \end{pmatrix}$, where j_{0x} and j_{0y} are the uniform current

components and δj_x and δj_y are the nonequilibrium current components. Then, Eq. (D1) can be written as

$$\mathbf{E} = \begin{pmatrix} \rho_0 & -\rho_H \\ \rho_H & \rho_0 \end{pmatrix} \begin{pmatrix} j_{0x} + \delta j_x \\ j_{0y} + \delta j_y \end{pmatrix}. \quad (\text{D2})$$

Then, the electrical field components E_x and E_y can be expressed as

$$E_x = \rho_0(j_{0x} + \delta j_x) - \rho_H(j_{0y} + \delta j_y), \quad (\text{D3})$$

$$E_y = \rho_H(j_{0x} + \delta j_x) + \rho_0(j_{0y} + \delta j_y). \quad (\text{D4})$$

Since the input current density is constant, the electrical field, \mathbf{E} , should satisfy the following conditions:

$$\nabla \times \mathbf{E} = \frac{\partial E_y}{\partial x} - \frac{\partial E_x}{\partial y} = 0. \quad (\text{D5})$$

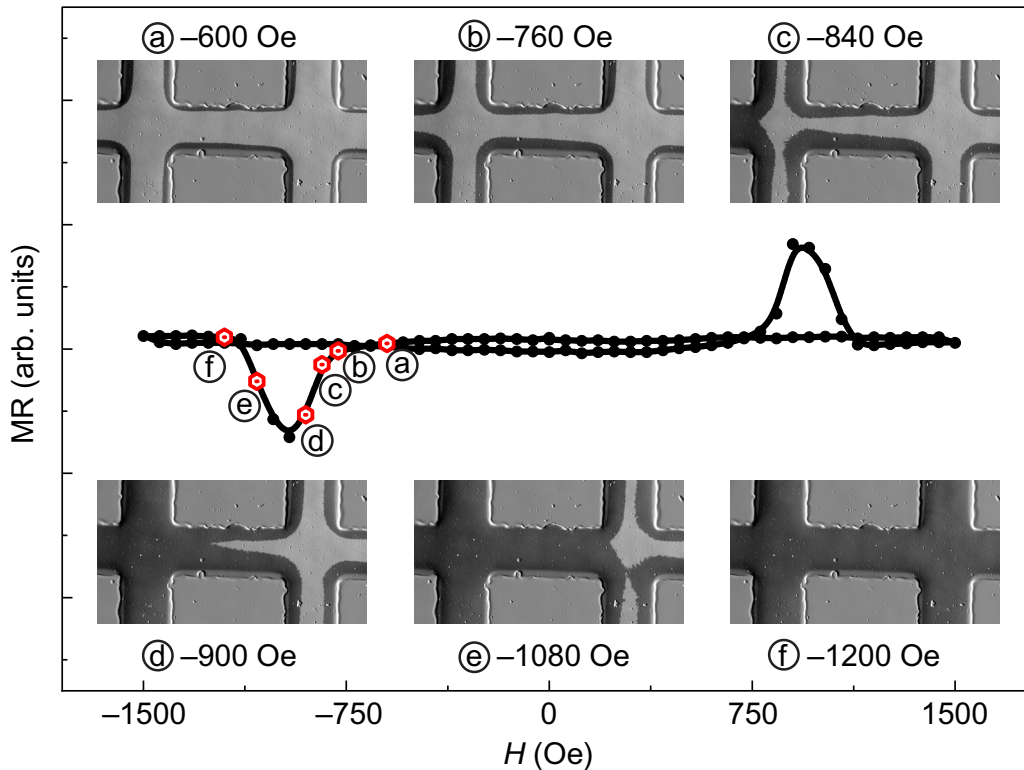


FIG. 8. Field dependence of asymmetric MR and simultaneously measured MOKE images of domain patterns at specified fields in descending-field branch.

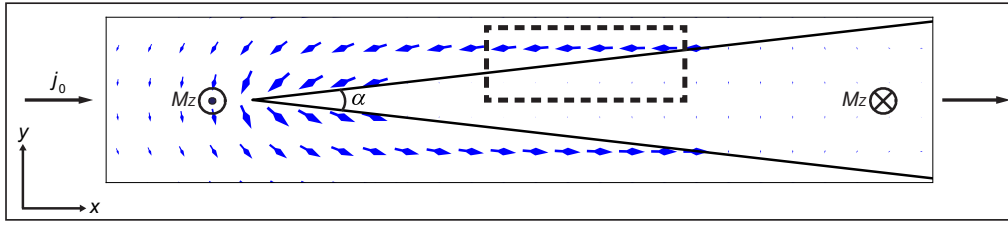


FIG. 9. Distribution of nonequilibrium currents in a rectangular-shaped film with tilting domain walls. α is the angle between tilting walls. Dashed line box indicates the integral path.

Substituting Eqs. (D3) and (D4) into Eq. (D5) yields

$$\frac{\partial[\rho_H(j_{0x} + \delta j_x) + \rho_0(j_{0y} + \delta j_y)]}{\partial x} = \frac{\partial[\rho_0(j_{0x} + \delta j_x) - \rho_H(j_{0y} + \delta j_y)]}{\partial y}. \quad (\text{D6})$$

Considering ρ_0 is constant and neglecting the second-order terms, Eq. (D6) can be simplified as

$$j_{0x} \frac{\partial \rho_H}{\partial x} + j_{0y} \frac{\partial \rho_H}{\partial y} = \rho_0 \left(\frac{\partial \delta j_x}{\partial y} - \frac{\partial \delta j_y}{\partial x} \right). \quad (\text{D7})$$

By multiplying unit vector $\hat{\mathbf{k}}$ on both sides, Eq. (D7) can be rewritten in the form

$$\left(j_{0x} \frac{\partial \rho_H}{\partial x} + j_{0y} \frac{\partial \rho_H}{\partial y} \right) \hat{\mathbf{k}} = -\rho_0 (\nabla \times \delta \mathbf{j}). \quad (\text{D8})$$

Considering that the uniform current, j_0 , flows along the x direction, we have $j_{0x} = j_0$ and $j_{0y} = 0$. Equation (D8) can be written as

$$j_0 \frac{\partial \rho_H}{\partial x} \hat{\mathbf{k}} = -\rho_0 (\nabla \times \delta \mathbf{j}). \quad (\text{D9})$$

In general, the Hall resistivity, ρ_H , in a ferromagnet is defined as

$$\rho_H = R_0 H + R_S M_Z, \quad (\text{D10})$$

where R_0 and R_S are the coefficients for the ordinary and anomalous Hall effects, respectively. H is the external magnetic field, and M_Z is the magnetization along the film's normal direction. Considering the fact that the ordinary Hall resistivity is negligible compared with the anomalous Hall resistivity in magnetic films with strong perpendicular magnetic anisotropy, by substituting Eq. (D10) into Eq. (D9), we get

$$\nabla \times \delta \mathbf{j} = -\frac{J_S R_S}{\rho_0} \frac{\partial M_z}{\partial x} \hat{\mathbf{k}}. \quad (\text{D11})$$

The calculated result clearly reveals that the inhomogeneous distribution of perpendicular magnetization, M_Z , along the x direction, more specifically, the tilting domain walls, gives rise to nonequilibrium current $\delta \mathbf{j}$.

2. Geometry factors affecting nonequilibrium current

As shown in Fig. 9, the angle between the tilting domain walls of the wedged domain is defined as α . Since the Hall electrical field can be expressed as $\mathbf{E}_H = \rho_H \mathbf{j}_0 = \begin{pmatrix} 0 & -\rho_H \\ \rho_H & 0 \end{pmatrix} \begin{pmatrix} j_{0x} \\ j_{0y} \end{pmatrix} = \begin{pmatrix} E_{Hx} \\ E_{Hy} \end{pmatrix}$, Eq. (D8) can be rewritten as

$$-\rho_0 (\nabla \times \delta \mathbf{j}) = \left(\frac{\partial E_{Hy}}{\partial x} - \frac{\partial E_{Hx}}{\partial y} \right) \hat{\mathbf{k}} = \nabla \times \mathbf{E}_H. \quad (\text{D12})$$

By choosing a box-loop integral (length, x_0 ; width, y_0) and applying Stokes theorem to both sides of Eq. (D12), we obtain

$$-\rho_0 \oint \delta \mathbf{j} \cdot d\mathbf{l} = \oint \mathbf{E}_H \cdot d\mathbf{l}. \quad (\text{D13})$$

Considering that the nonequilibrium current is only valid near the upper edge of the tilting wall in the integral loop and the Hall electrical field, E_H , is along the y direction, we get the following relations:

$$\rho_0 x_0 |\delta \mathbf{j}| = 2x_0 \tan \frac{\alpha}{2} E_H = 2x_0 \tan \frac{\alpha}{2} \rho_H j_0. \quad (\text{D14})$$

Thus, the nonequilibrium current, $|\delta \mathbf{j}|$, inside the integral region can be expressed as

$$|\delta \mathbf{j}| = 2j_0 (\rho_H / \rho_0) \tan \frac{\alpha}{2}. \quad (\text{D15})$$

Therefore, the nonequilibrium current is dominated by the geometry factor, $\tan(\alpha/2)$, which is determined jointly by sample geometry, magnetic anisotropy of the film, and the inhomogeneous field gradient in the real scenario.

-
- [1] T. McGuire and R. Potter, Anisotropic magnetoresistance in ferromagnetic 3d alloys, *IEEE Trans. Magn.* **11**, 1018 (1975).
 - [2] I. A. Campbell and A. Fert, *Ferromagnetic Materials* (North-Holland, Amsterdam, 1982).
 - [3] M. N. Baibich, J. M. Broto, A. Fert, F. Nguyen Van Dau, F. Petroff, P. Etienne, G. Creuzet, A. Friederich, and J. Chazelas, Giant Magnetoresistance of (001)Fe/(001)Cr Magnetic Superlattices, *Phys. Rev. Lett.* **61**, 2472 (1988).

- [4] S. S. Parkin, N. More, and K. P. Roche, Oscillations in Exchange Coupling and Magnetoresistance in Metallic Superlattice Structures: Co/Ru, Co/Cr, and Fe/Cr, *Phys. Rev. Lett.* **64**, 2304 (1990).
- [5] M. Julliere, Tunneling between ferromagnetic-films, *Phys. Lett. A* **54**, 225 (1975).
- [6] J. S. Moodera and L. R. Kinder, Ferromagnetic–insulator–ferromagnetic tunneling: Spin-dependent tunneling and large magnetoresistance in trilayer junctions (invited), *J. Appl. Phys.* **79**, 4724 (1996).
- [7] P. M. Levy and S. Zhang, Resistivity Due to Domain Wall Scattering, *Phys. Rev. Lett.* **79**, 5110 (1997).
- [8] R. P. van Gorkom, A. Brataas, and G. E. W. Bauer, Negative Domain Wall Resistance in Ferromagnets, *Phys. Rev. Lett.* **83**, 4401 (1999).
- [9] A. Brataas, G. Tatara, and G. E. W. Bauer, Ballistic and diffuse transport through a ferromagnetic domain wall, *Phys. Rev. B* **60**, 3406 (1999).
- [10] C. H. Marrows, Spin-polarised currents and magnetic domain walls, *Adv. Phys.* **54**, 585 (2005).
- [11] H. X. Tang, S. Masmanidis, R. K. Kawakami, D. D. Awschalom, and M. L. Roukes, Negative intrinsic resistivity of an individual domain wall in epitaxial (Ga, Mn)As microdevices, *Nature* **431**, 52 (2004).
- [12] X. M. Cheng, S. Urazhdin, O. Tchernyshyov, C. L. Chien, V. I. Nikitenko, A. J. Shapiro, and R. D. Shull, Antisymmetric Magnetoresistance in Magnetic Multilayers with Perpendicular Anisotropy, *Phys. Rev. Lett.* **94**, 017203 (2005).
- [13] G. Xiang, A. W. Holleitner, B. L. Sheu, F. M. Mendoza, O. Maksimov, M. B. Stone, P. Schiffer, D. D. Awschalom, and N. Samarth, Magnetoresistance anomalies in (Ga, Mn)As epilayers with perpendicular magnetic anisotropy, *Phys. Rev. B* **71**, 241307 (2005).
- [14] W. Desrat, S. Kamara, F. Terki, S. Charar, J. Sadowski, and D. K. Maude, Antisymmetric magnetoresistance anomalies and magnetic domain structure in GaMnAs/InGaAs layers, *Semicond. Sci. Technol.* **24**, 065011 (2009).
- [15] D. L. Partin, M. Karnezos, L. C. deMenezes, and L. Berger, Nonuniform current distribution in the neighborhood of a ferromagnetic domain wall in cobalt at 4.2 K, *J. Appl. Phys.* **45**, 1852 (1974).
- [16] L. Berger, Low-field magnetoresistance and domain drag in ferromagnets, *J. Appl. Phys.* **49**, 2156 (1978).
- [17] G. Xiang and N. Samarth, Theoretical analysis of the influence of magnetic domain walls on longitudinal and transverse magnetoresistance in tensile strained (Ga, Mn)As epilayers, *Phys. Rev. B* **76**, 054440 (2007).
- [18] A. Segal, O. Shaya, M. Karpovskii, and A. Gerber, Asymmetric field dependence of magnetoresistance in magnetic films, *Phys. Rev. B* **79**, 144434 (2009).
- [19] Z. Liu, S. M. Zhou, and X. B. Jiao, Correlation between perpendicular magnetic anisotropy and microstructure in TbFeCo and TbFeCo–SiO₂ films, *J. Phys. D: Appl. Phys.* **42**, 015008 (2009).
- [20] R. Moubah, F. Magnus, B. Hjörvarsson, and G. Andersson, Antisymmetric magnetoresistance in SmCo₅ amorphous films with imprinted in-plane magnetic anisotropy, *J. Appl. Phys.* **115**, 053911 (2014).
- [21] S. Singh, M. A. Basha, C. L. Prajapat, H. Bhatt, Y. Kumar, M. Gupta, C. J. Kinane, J. Cooper, M. R. Gonal, S. Langridge, and S. Basu, Antisymmetric magnetoresistance and helical magnetic structure in a compensated Gd/Co multilayer, *Phys. Rev. B* **100**, 140405 (2019).
- [22] J. Finley and L. Liu, Spin-Orbit-Torque Efficiency in Compensated Ferrimagnetic Cobalt-Terbium Alloys, *Phys. Rev. Appl.* **6**, 054001 (2016).
- [23] S. N. Gadetsky, A. V. Stupnov, M. V. Zumkin, and E. N. Nikolaev, Domain-Wall dynamics in tbfeCo thin-films, *IEEE Trans. Magn.* **28**, 2928 (1992).
- [24] Y. Yafet and E. M. Gyorgy, Ferromagnetic strip domains in an atomic monolayer, *Phys. Rev. B: Condens. Matter Mater. Phys.* **38**, 9145 (1988).
- [25] H. Alex and S. Rudolf, *Magnetic Domains* (Springer-Verlag, Berlin, Heidelberg, 1998).
- [26] S. Alebrand, U. Bierbrauer, M. Hehn, M. Gottwald, O. Schmitt, D. Steil, E. E. Fullerton, S. Mangin, M. Cinchetti, and M. Aeschlimann, Subpicosecond magnetization dynamics in TbCo alloys, *Phys. Rev. B* **89**, 144404 (2014).
- [27] M. T. Rahman, L. Xiaoxi, M. Matsumoto, and A. Morisako, Compositional dependence of magnetoresistance in TbFeCo amorphous film, *IEEE Trans. Magn.* **41**, 2568 (2005).